Microwave Remote Sensing of Ionized Air

S. Liao, N. Gopalsami, A. Heifetz, T. Elmer, P. Fiflis, E. R. Koehl, H. T. Chien, and A. C. Raptis

Abstract—We present observations of microwave scattering from ambient room air ionized with a negative ion generator. The frequency dependence of the radar cross section of ionized air was measured from 26.5 to 40 GHz (Ka-band) in a bistatic mode with an Agilent PNA-X series (model N5245A) vector network analyzer. A detailed calibration scheme is provided to minimize the effect of the stray background field and system frequency response on the target reflection. The feasibility of detecting the microwave reflection from ionized air portends many potential applications such as remote sensing of atmospheric ionization and remote detection of radioactive ionization of air.

Index Terms—Electromagnetic reflection, electromagnetic scattering, radar cross section (RCS), radar scattering.
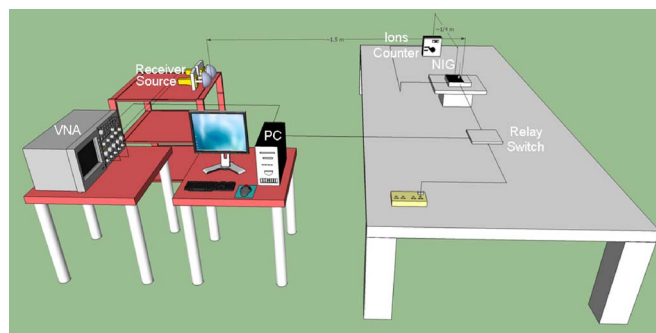

Fig. 1. Experimental setup for microwave reflection measurement of ionized air: An Agilent PNA-X series (Model N5245A) VNA sweeps the frequency over the Ka-band (26.5–40 GHz), a pair of lens-coupled horns is used to transmit/receive radiation in open air, a computer-controlled relay switch turns the NIG on and off to ionize air, and an ion counter is used to monitor the charge density.

I. INTRODUCTION

MICROWAVE remote sensing of Earth resources and weather has been extensively studied in the past [1]–[6]. However, there has been limited work on microwave remote sensing of ionized air in spite of its importance in atmospheric physics. Remote sensing of ionized air has many potential applications in atmospheric sciences and national security. Our group has recently investigated microwave scattering from charged dielectric cylinders [7] and charged water droplets [8]. In this letter, we report observations of microwave scattering from ambient room air ionized with a negative ion generator (NIG). Measurements of the radar cross section (RCS) of ionized air were made in the Ka-band (26.5 to 40 GHz) with a vector network analyzer (VNA) in a bistatic mode whose low noise floor $(< -100 \text{ dB})$ enables the detection of weak signals.

This letter is organized as follows. The experimental setup and procedure for the RCS measurement of ionized air are presented in Section II, followed by a discussion of the test results in Section III, plausible explanations in Section IV, and conclusions in Section V.

II. EXPERIMENTAL MEASUREMENTS

A. Description of Laboratory Setup

A schematic drawing of the experimental setup is shown in Fig. 1. A NIG is used to generate ionized air on the order of 1 million negative ions/cm^3 at a distance of about 40 cm

from the NIG needle. The ion density depends on the distance from the NIG needle, which is biased at -18 kV. To perform microwave scattering measurements, an Agilent PNA-X series (Model N5245A) VNA was used to sweep the frequency and record the network scattering parameter S_{21} from 26.5 to 40 GHz (Ka-band). A pair of Ka-band standard gain rectangular horn antennas (Narda Microwave-East) was used for the emission and detection of microwaves. Dielectric lenses were used with each horn antenna to increase the gain of the antenna radiation pattern. A computer-controlled relay switch was used to turn the NIG on and off, which allowed for making time-gated transient measurements. The emitter and receiver antennas were placed side by side for bistatic mode detection. The two antennas were separated by a distance of 30 cm to reduce electromagnetic coupling, and each was focused at the tip of the NIG needle which is approximately 1.5 m away. The S_{21} signal was collected by the VNA and transferred to a personal computer through a general-purpose interface bus. A LabVIEW graphical user interface data acquisition program was used to view the experimental observations in real time.

B. System Calibration

The VNA can be calibrated at an arbitrary reference plane in a closed cable system using the short-open-load-through calibration method [9]–[11]. However, in our experiment, the VNA was used to interrogate an open air space between two antennas, where one must take into account the stray fields due to the coupling of the emitter and receiver antenna signals and the background reflection. Furthermore, the frequency response of the entire measurement system must be known to determine the absolute RCS.

For a plane wave that is incident upon an infinite dielectric slab of thickness t, the RCS for an incident beam area of $A = \pi a^2$ is related to the power reflection coefficient (PRC) as

$$RCS = A \times PRC = \frac{AP_r}{P_i} = A\left|\frac{E_r}{E_i}\right|^2 = A|r|^2 = AR \quad (1)$$

where P_i and P_r are the incident and reflected power, respectively, E_i and E_r are the corresponding fields, and r and R are the voltage reflection coefficient and PRC, respectively. However, due to the background field and frequency response of the system previously stated, the S_{21} signal measured at the VNA is given by

$$S_{21} = [E_b + E_r]T(f) = E_i[r_b + r]T(f) \quad (2)$$

where E_i is the complex incident plane-wave field, E_b is the background stray field, r_b is the complex reflection coefficient of the background, r is the reflection coefficient of interest that must be recovered from the signal S_{21}, and $T(f)$ is the frequency response of the system. From (2), the true reflection coefficient is obtained as

$$r = \frac{S_{21} - S_{21}^b}{E_i T(f)} \quad (3)$$

where $S_{21}^b = E_i r_b T(f)$ is the measured background signal when the NIG is off. To obtain $E_i T(f)$, we placed a large piece of metal reflector at the center position of ionized air, which has reflection $r = -1$ for all frequencies. Let S_{21}^m denote the measurement data from the metal reflector. From (2), we have

$$S_{21}^m = E_i[r_b - 1]T(f) \quad (4)$$

from which we have

$$E_i T(f) = S_{21}^b - S_{21}^m. \quad (5)$$

Combining (3) and (5), we obtain the calibrated reflection coefficient

$$r = \frac{S_{21} - S_{21}^b}{S_{21}^b - S_{21}^m}. \quad (6)$$

From (1) and (6), we obtain the RCS per square meter

$$RCS = \frac{A \times PRC}{A}(m^2) = \left|\frac{S_{21} - S_{21}^b}{S_{21}^m - S_{21}^b}\right|^2 (m^2) \quad (7)$$

and the RCS per volume is given by

$$\frac{RCS}{volume} = \frac{A \times PRC}{A \times t} = \frac{1}{t}\left|\frac{S_{21} - S_{21}^b}{S_{21}^m - S_{21}^b}\right|^2. \quad (8)$$

The calibration procedure may be summarized as follows.

1) Make a measurement when the NIG is off, and denote it as S_{21}^b.
2) Make another measurement by putting a large piece of metal at the position of the ionized air, and denote it as S_{21}^m.
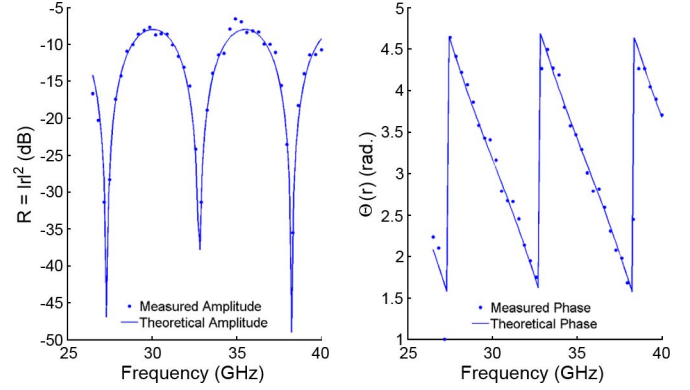

Fig. 2. Measured amplitude and phase of reflection coefficient for 18-mm-thick Teflon slab along with theoretical comparisons based on (9).

3) Make ionized air measurements with the NIG turned on and off, and denote it as S_{21}.
4) Perform the RCS calibration as in (7) and (8).

To validate our calibration technique on a known target, we performed the calibration on a Teflon slab of thickness $t = 18$ mm and compared it with the theoretical result. For plane-wave normal incidence, the reflection coefficient r_{Teflon} is

$$r_{\text{Teflon}} = \frac{\left[\frac{1}{\varepsilon_{\text{Teflon}}} - 1\right]\left[1 - \exp(-j2k_{\text{Teflon}}t)\right]}{\left[\frac{1}{\sqrt{\varepsilon_{\text{Teflon}}}} + 1\right]^2 - \left[\frac{1}{\sqrt{\varepsilon_{\text{Teflon}}}} - 1\right]^2 \exp(-j2k_{\text{Teflon}}t)} \quad (9)$$

where $\varepsilon_{\text{Teflon}} = 2.3215$ and k_{Teflon} are the dielectric constant and wave vector of Teflon, respectively. A good agreement between the theoretical and measured data is obtained as shown in Fig. 2.

III. EXPERIMENTAL RESULTS

In this section, we present the experimental data of the RCS per square meter obtained from (7) of the ionized air when the NIG is on and off for three cycles. Another interesting quantity, the RCS per volume, can be obtained through (8), with $t \sim 1/4$ m (twice the radius of the ionized air).

The measured RCS per square meter in the Ka-band (26.5–40 GHz) is shown in Fig. 3 for three cycles when the NIG is on and off. Clearly, when the ionized air is present, the RCS per square meter increases and is on the order of $10^{-5} - 10^{-4}$ m^2 over the whole band. This level of RCS per square meter can be easily detected by current radar systems.

If we average the difference in the RCS per square meter between when the NIG is on and when the NIG is off for three cycles, the averaged RCS per square meter in the Ka-band is shown in Fig. 4.

IV. DISCUSSION

Whereas microwave radar is known to detect highly dense charged columns of air from lightning, meteors, etc., due to a higher plasma frequency than the incident radar frequency
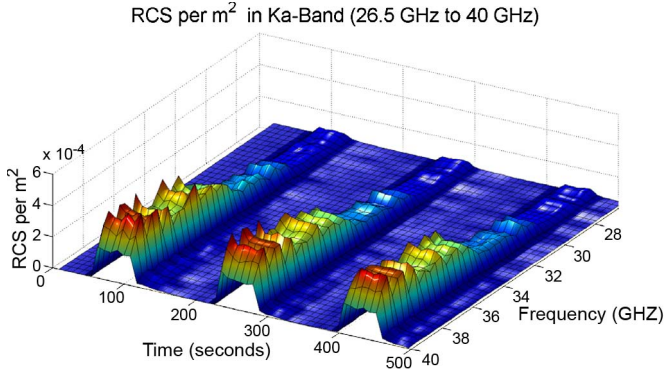
Fig. 3. Measured RCS per square meter in the Ka-band (26.5–40 GHz) for three cycles when the NIG is on and off.

Fig. 5. Calculated RCS per square meter for an electron density distribution of $10^6|z|^{-\delta}/\mathrm{cm}^3$ according to (13).
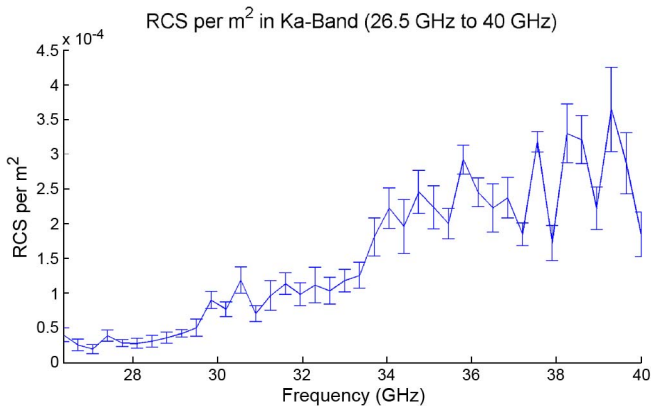

Fig. 4. Averaged RCS per square meter in the Ka-band (26.5–40 GHz): The error bars show the standard deviation of the RCS per square meter.

[12], there have only been limited studies on radar detection of weakly ionized air [13]. We have identified two plausible mechanisms that may explain the microwave interaction of air ionization: 1) coherent Thomson scattering from free electrons released from ionization and 2) scattering from charged water microdroplets as they may form from ion-nucleated water clustering [14]. We have analyzed the latter case—the millimeter-wave scattering from charged microdroplets—in an earlier study [8]. While the charged droplet scattering may be the case in atmospheric air, we believe that the coherent Thomson scattering might explain the present measurements in room air.

Thomson scattering arises from the acceleration of free electrons by the incident electric field. The electron density in the ionized air is on the order of $\bar{n}_e \sim 10^6/\mathrm{cm}^3$, which gives an average spacing between adjacent electrons of $d_e \sim 0.0022$ cm, which is much smaller than the wavelength of $\lambda = 1$ cm at a frequency of $f = 30$ GHz. In this case, i.e., within one wavelength scale, the scattered field for a unit plane-wave incidence is given by

$$\vec{E}_s = s_e \int_V \bar{n}_e(\vec{r}) \exp\left(-j2[\vec{k}_s - \vec{k}_i] \bullet \vec{r}\right) d\vec{r} \quad (10)$$

where s_e is the single-electron scattering strength, $\sigma_T = |s_e|^2 = 6.65 \times 10^{-29}$ m^2 is the Thomson scattering of a single
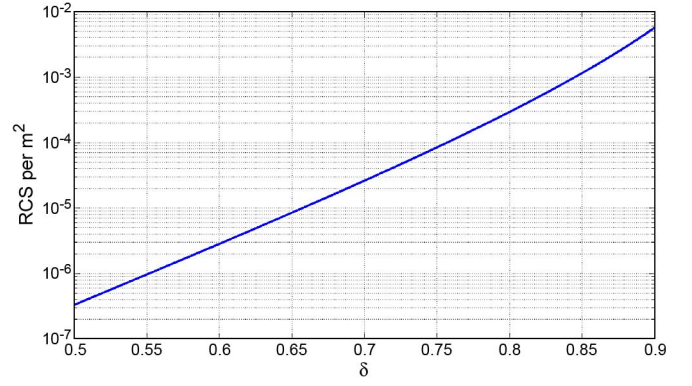
electron, and $\vec{k}_s$ and $\vec{k}_i$ are the scattered and incident wave vectors, respectively. The time-averaged backscattered RCS for weakly ionized air is given by [12]

$$RCS = |\vec{E}_s|^2 = \sigma_T \left| \int_V \bar{n}_e(\vec{r}) \exp\left(-j2[\vec{k}_s - \vec{k}_i] \bullet \vec{r}\right) d\vec{r} \right|^2 . \quad (11)$$

Thus, the total scattering depends quadratically on the Fourier transform component of the electron density profile. As a rough order of magnitude, we evaluate the time-averaged backscattering RCS $(|\vec{k}_s - \vec{k}_i| = 2k)$ for an assumed electron density distribution of

$$\bar{n}_e(z) = \bar{n}_e|z|^{-\delta}, \qquad \delta \in [0, 1) \quad (12)$$

in which case the RCS becomes

$$RCS = \sigma_T[\bar{n}_e]^2 \left| 2^\delta k^{\delta-1} \frac{\sqrt{\pi}\Gamma\left(\frac{1-\delta}{2}\right)}{2^\delta \Gamma\left(\frac{\delta}{2}\right)} \right|^2 m^2 \quad (13)$$

where Γ is the Gamma function. Fig. 5 shows the calculated RCS according to (13) over a range of δ's, which agrees well with the measured RCS in Fig. 4.

V. CONCLUSION

We have observed microwave reflection from ionized air using the NIG as the source of ionization. An RCS on the order of $10^{-5} - 10^{-4}$ m^2 was measured over the whole Ka-band (26.5–40 GHz) in room air for a charge density of ~ 1 million/ cm^3 at a distance of 40 cm from the NIG needles. We have surmised coherent Thomson scattering as a plausible detection mechanism. This is a significant result from the standpoint of remote sensing of nuclear sources, which is from their ionization of air. The detection of charges from nuclear materials or radioactive plumes allows for remote sensing of nuclear proliferation events. Additionally, the detection of the RCS of ionized air can shed light on the understanding of cloud and rain formation and in early monitoring of thunderstorms.

REFERENCES

[1] S. Tanelli, S. L. Durden, and E. Im, "Simultaneous measurements of Ku- and Ka-band sea surface cross sections by an airborne radar," *IEEE Geosci. Remote Sens. Lett.*, vol. 3, no. 3, pp. 359–363, Jul. 2006.

[2] J. B. Mead, A. L. Pazmany, S. M. Sekelsky, and R. E. Mcintosh, "Millimeter-wave radars for remotely sensing clouds and precipitation," *Proc. IEEE*, vol. 82, no. 12, pp. 1891–1906, Dec. 1994.

[3] W. T. Crow and X. Zhan, "Continental-scale evaluation of remotely-sensed soil moisture products," *IEEE Geosci. Remote Sens. Lett.*, vol. 4, no. 3, pp. 451–455, Jul. 2007.

[4] W. G. Stevens, D. J. McLaughlin, M. J. Sowa, B. Weijers, and X. Zhang, "Bistatic scattering behavior of forested hills at grazing incidence," *Electron. Lett.*, vol. 37, no. 12, pp. 783–784, Jun. 2001.

[5] D. W. Draper and D. G. Long, "Simultaneous wind and rain retrieval using sea winds data," *IEEE Trans. Geosci. Remote Sens.*, vol. 42, no. 7, pp. 1411–1423, Jul. 2004.

[6] I. S. Ashcraft and D. G. Long, "Observation and characterization of radar backscatter over Greenland," *IEEE Trans. Geosci. Remote Sens.*, vol. 43, no. 2, pp. 225–237, Feb. 2005.

[7] N. Gopalsami, H. T. Chien, A. Heifetz, E. R. Keohl, and A. C. Raptis, "Millimeter wave detection of nuclear radiation: An alternative detection mechanism," *Rev. Sci. Instrum.*, vol. 80, no. 8, p. 084702, Aug. 2009.

[8] A. Heifetz, H. T. Chien, S. Liao, N. Gopalsami, and A. C. Raptis, "Millimeter wave scattering from neutral and charged water droplets," *J. Quant. Spectrosc. Radiat. Transf.*, vol. 111, no. 17/18, pp. 2550–2557, Nov. 2010.

[9] J. A. Jargon, R. B. Marks, and D. K. Rytting, "Robust SOLT and alternative calibrations for four-sampler vector network analyzers," *IEEE Trans. Microw. Theory Tech.*, vol. 47, no. 10, pp. 2008–2013, Oct. 1999.

[10] H. J. Eul and B. Schiek, "A generalized theory and new calibration procedures for network analyzer self-calibration," *IEEE Trans. Microw. Theory Tech.*, vol. 39, no. 4, pp. 724–731, Apr. 1991.

[11] K. J. Silvonen, "A general approach to network analyzer calibration," *IEEE Trans. Microw. Theory Tech.*, vol. 40, no. 4, pp. 754–759, Apr. 1992.

[12] P. W. Gorham, "On the possibility of radar echo detection of ultra-high energy cosmic ray- and neutrino-induced extensive air showers," *Astropart. Phys.*, vol. 15, no. 2, pp. 177–202, Apr. 2001.

[13] S. V. Shevkunov, "Scattering of centimeter radiowaves in a gas ionized by radioactive radiation: Cluster plasma formation," *J. Exp. Theoretical Phys.*, vol. 92, no. 3, pp. 420–440, Mar. 2001.

[14] R. G. Harrison and K. S. Carslaw, "Ion–aerosol–cloud processes in the lower atmosphere," *Rev. Geophys.*, vol. 41, no. 3, p. 1012, 2003.